

# Determination of the friction law parameters of the Mw 6.7 Michilla earthquake in northern Chile by dynamic inversion

Sergio Ruiz<sup>1,2</sup> and Raul Madariaga<sup>1</sup>

Received 16 February 2011; revised 1 April 2011; accepted 1 April 2011; published 14 May 2011.

[1] We perform a full dynamic inversion at low frequencies of the 16 December 2007 (Mw = 6.7) northern Chile earthquake that we model as a simple elliptical patch. We use two different stress-friction end-member models: asperities and barriers, finding similar results. The inversions are performed for strong motion data filtered between 0.02 and 0.5 Hz. Eleven geometrical and stress and friction parameters are inverted using the neighbourhood algorithm. The optimum solutions have relative errors lower than 0.21. The earthquake rupture has duration of less than 5 s and propagates at sub-shear speed. The rupture area is similar to that of the aftershock distribution and the seismic moment is  $0.95 \cdot 10^{19}$  Nm. We derive the friction law parameters from the models situated close to the optimum solution using a Monte Carlo technique. The results show a strong trade-off between applied stress and frictional resistance. We find that the distribution of friction models collapses into a finite zone of the space of moment and non-dimensional parameter  $\kappa$ . We conclude that it is possible to determine the friction law from near field seismograms, but there is a strong trade-off between friction and initial stress. **Citation:** Ruiz, S., and R. Madariaga (2011), Determination of the friction law parameters of the Mw 6.7 Michilla earthquake in northern Chile by dynamic inversion, *Geophys. Res. Lett.*, 38, L09317, doi:10.1029/2011GL047147.

## 1. Introduction

[2] Full dynamic inversions of seismic sources are scarce because of the limited number of well recorded earthquake and the large computational resources required. With few exceptions, dynamic inversion of earthquake rupture has been done in two steps. First a kinematic inversion is done and, then, stresses and strength are computed by dynamic modelling [e.g., *Fukuyama and Mikumo*, 1993; *Bouchon et al.*, 1998]. However, the approximations made in kinematic source models, affect the inferred dynamic parameters [*Guatteri and Spudich*, 2000; *Piatanesi et al.*, 2004], propagating errors from the kinematic inversion to the dynamic simulation. In addition, dynamic inversion is intrinsically non unique as was discussed by *Peyrat et al.* [2001]. Two end-models of the earthquake source heterogeneity can be used in the inversion: the barrier [*Das and Aki*, 1977] and asperity [*Kanamori and Stewart*, 1978] models. Although similar radiation is predicted for these two models [*Madariaga*, 1979], only in the partial dynamic inversion of the 1992 Landers

earthquake has it been possible to test this hypothesis with strong motion data [*Peyrat et al.*, 2001].

[3] *Peyrat and Olsen* [2004] did a full dynamic inversion of the 2000 Tottori earthquake using a classical discretisation of the fault into rectangles with constant stress and rupture resistance. *Di Carli et al.* [2010] improved these results using a stress distribution described by a few elliptical patches. Because of limited resolution and computer resources *Di Carli et al.* [2010] could not completely invert for the parameters of the friction law.

[4] Here we do a full dynamic inversion of the Michilla, northern Chile, earthquake of 16 December 2007. This Mw 6.7 event was an intraplate intermediate depth earthquake recorded by strong motion, broad band and short period instruments. These high quality data allow us to invert for the parameters of stress, the friction law, and the geometry and location of the rupture area, in total 11 parameters. The search for the best solutions are made using the Neighbourhood algorithm (NA) [*Sambridge*, 1999], and once an optimum solution is found by NA, we use the Montecarlo method (MC) to explore the initial stress field and the friction law.

## 2. The Michilla Earthquake

[5] The 16 December 2007 Northern Chile earthquake occurred inside the subducted Nazca plate at 43 km depth with an epicenter at 22.98°S, 70.24°W near the town of Michilla in the southern part of the rupture area of the Mw 7.8 Tocopilla earthquake of 2007 [*Delouis et al.*, 2009; *Peyrat et al.*, 2010]. *Peyrat et al.* [2010] performed a kinematic inversion of this event finding that the earthquake could be modeled as a simple elliptical shear fault with seismic moment of  $2.14 \times 10^{19}$  Nm (Mw = 6.8). The slab-push type rupture propagated along an almost vertical fault plane (strike 4°N, dip 85°, rake 90°) (Figure 1). The aftershocks of the Michilla earthquake were distributed along the fault plane covering an ellipsoidal zone less than 10 kilometres of radio centered on the hypocenter of the event (A. Fuenzalida et al., manuscript in preparation, 2011) (Figure 1).

[6] This earthquake was very well recorded by short period, broad band and strong motion instruments [*Sobiesiak et al.*, 2008; *Schurr et al.*, 2009; R. Boroschek et al., Terremoto Norte Chile, 14 Noviembre de 2007 M = 7.7, available from <http://www.terremotosuchile.cl>]. For the inversion we used two types of strong motion data: Episensor FBA ES-T continuously recording accelerometers at 100 Hz with 24 bit digitizers; and triggered instruments, mostly Kinematics ETNA with 24 bit Episensor digitizers at 200 Hz (<http://www.terremotosuchile.cl>). The strong motion data are baseline corrected and filtered using a band-pass causal Butterworth filter of order 4, and then integrated twice. The synthetic time

<sup>1</sup>Laboratoire de Géologie, Ecole Normale Supérieure, Paris, France.

<sup>2</sup>Departamento de Geología, Universidad de Chile, Santiago, Chile.

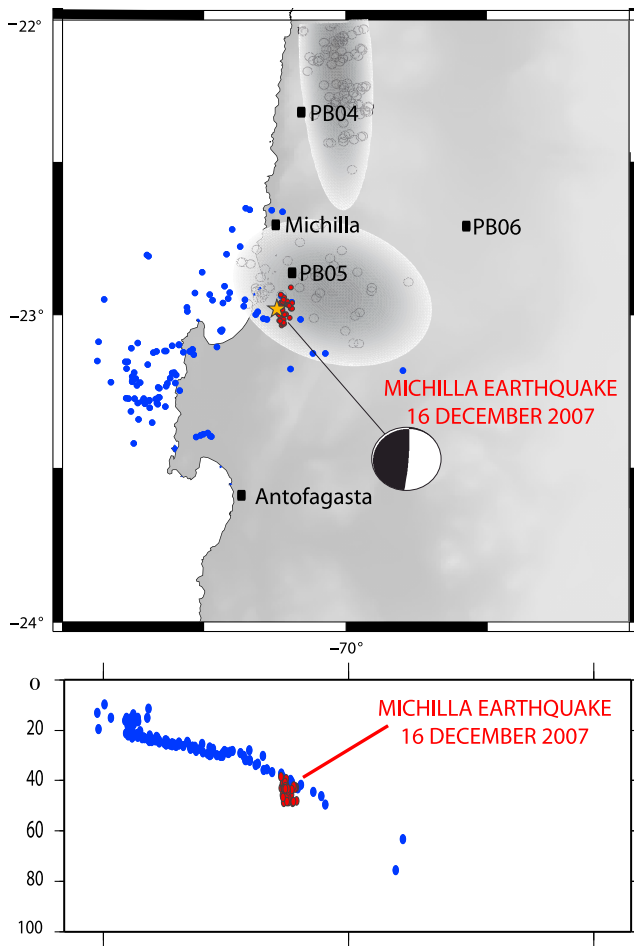


**Figure 1.** Location of the Michilla earthquake of 16 December 2007 in Northern Chile. This is a slab push event situated inside the subducted Nazca plate, immediately below the rupture zone of the Tocopilla earthquake of 14 November 2007. The grey ellipses show the slip areas determined by *Peyrat et al.* [2010] for the main event of 14 November 2007. Black squares are the locations of the strong motion instruments used in this work. The relocated events of 16 December 2007 are shown in red and the events from 13 to 16 December 2007 with blue colour (*Fuenzalida et al.*, manuscript in preparation, 2011).

series obtained from inversion are filtered in the same way. The corner frequency of the lowpass filter was chosen as 0.02 Hz because some records were triggered and had durations of only 100 seconds. We chose a highpass corner frequency of 0.5 Hz, because above this frequency site effects

or reflections in shallow strata are not well reproduced by the 1D velocity model that we used [*Husen et al.*, 1999]. Although, we tested all the strong motion records available, we worked with the 5 records shown in Figure 1 because they have the highest signal to noise ratio.

### 3. Dynamic Inversion Method

[7] In the forward dynamic problem we assumed that rupture occurred inside a flat elliptical patch. We assumed that stress and friction were uniform inside the fault because we are looking for the average properties of the rupture. Rupture propagation was controlled by the slip-weakening friction law proposed by *Ida* [1972]:

$$T_f(D) = T_u \left(1 - \frac{D}{D_c}\right) \quad D < D_c \quad (1)$$

$$T_f(D) = 0 \quad D > D_c$$

where  $T_f$  is friction as a function of slip  $D$ .  $T_u$  is the peak frictional stress or strength and  $D_c$  is the slip weakening distance. In (1) a constant kinematic friction should be added, for simplicity we assumed that it was equal to 0. Other versions of slip weakening friction [see, e.g., *Bizzarri*, 2009] can be used but we do not think that our observations can distinguish among them.

[8] The elliptical patch is described by 5 parameters, two for the principal semi-axis ( $a$  and  $b$ ), two for the position of the ellipse with respect to the hypocenter ( $X$ ,  $Y$ ) and the angle of the principal axis. As shown in Table 1 the range of variation of geometrical parameters was sufficiently broad so that a large set of potential elliptical ruptures were explored in the inversion. For rupture initiation we followed the methodology of *Madariaga and Olsen* [2000] assuming that rupture was triggered by a small circular asperity of radius  $R'$  inside of the ellipse, with strength  $T'_c$  that is higher than the peak frictional stress  $T_u$ . We inverted both for  $R'$  and  $T'_c$ . Once rupture breaks the small asperity, it can grow or stop spontaneously depending on the values of the stress field ( $T_e$ ) and the friction law. In our model we assumed that stress and friction were constant inside the elliptical rupture zone. As shown in Table 1, we explored 4 stress parameters: the slip-weakening distance  $D_c$  and yield stress  $T_u$  of the friction law (1), and the external applied stress  $T_e$ . Outside the ellipse, stress and friction depend on the rupture model. For the asperity model [*Kanamori and Stewart*, 1978], the region outside the ellipse was considered to have a negative initial stress load  $T_{out}$  so that rupture stopped when it reached this region of reduced initial stress. For the barrier model [*Das and Aki*, 1977] the yield stress outside the rupture zone was

**Table 1.** Values of the 11 Inverted Parameters for the Asperity and Barrier Models<sup>a</sup>

Model	Geometry					Nucleation		Stress			
	Semi Axis a [Km]	Semi Axis b [Km]	X [Km]	Y [Km]	Angle [rad]	$R'$ [Km]	$T'_c$ [Mpa]	$T_e$ [Mpa]	$T_u$ [Mpa]	$D_c$ [m]	$T_{out}$ [Mpa]
Asperity	4.00	10.12	0.85	-2.00	1.50	0.98	23.65	14.97	19.18	0.65	-108.4
Barrier	4.23	12.42	0.28	-2.00	0.07	1.00	14.74	10.89	12.82	0.56	130.1
Range minimum	4	4	-2	-2	0	0.8	8	8	8	0.4	-8
Range maximum	14	14	2	2	1.57	2	120	50	100	2	1800

<sup>a</sup>The optimal values are on the first two lines and the ranges of variation of these parameters during the inversion are shown in the last two lines.

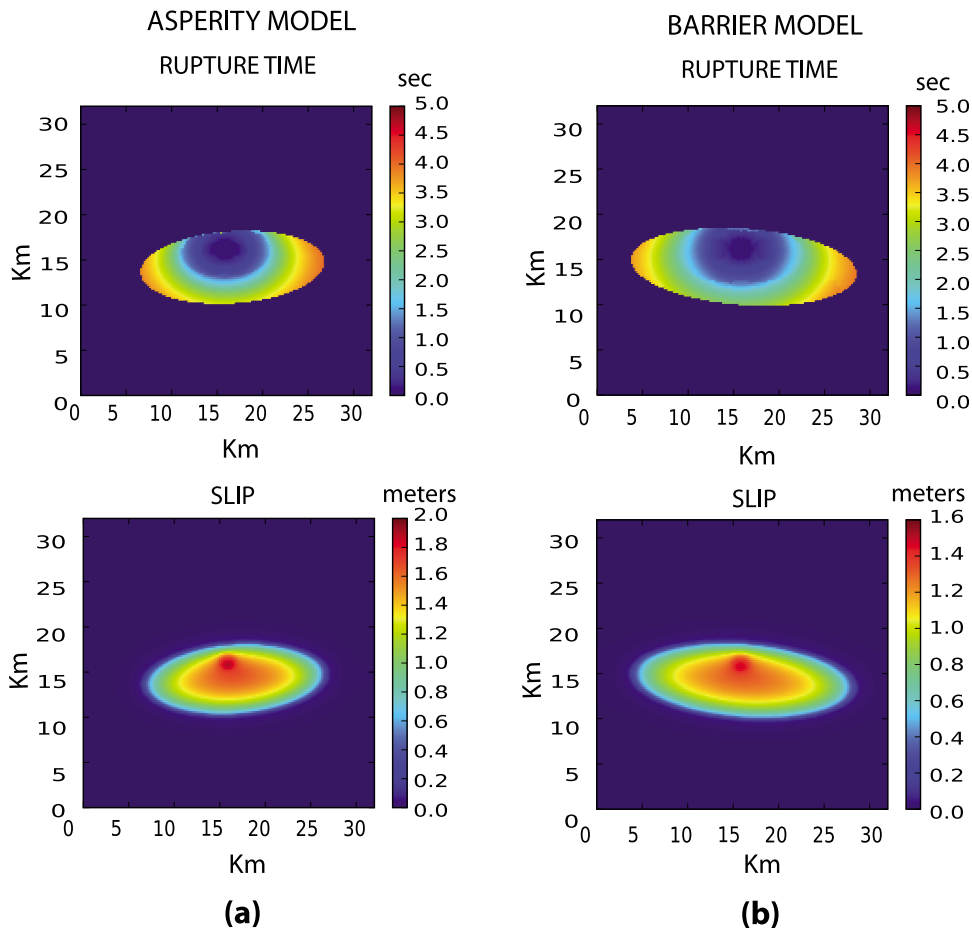


**Figure 2.** Slip and rupture isochrones for the 2007 Michilla earthquake of Northern Chile. The top figures show the rupture time and the lower figures the slip distribution of the best (a) asperity and (b) barrier model. The total moment for both models is  $1 \cdot 10^{19}$  Nm and duration is 4.5 s for both models.

a very large positive  $T_{\text{out}}$  constant, so that rupture stops because friction becomes very large. The 11 parameters were inverted independently for the asperity and barrier models.

[9] A 3D fourth-order staggered-grid finite differences method with absorbing boundaries and thin fault boundary conditions was used to solve the forward dynamic rupture simulation [Madariaga *et al.*, 1998]. The spatial and temporal discretisations were 200 m and 0.005 s respectively. The grid had  $160 \times 160 \times 160$  elements and was centered at the hypocenter on the fault plane. The fault zone is 32 km wide and 32 km deep but only a small part broke during the earthquake. The AXITRA code [Coutant, 1990; Bouchon, 1981] was used to simulate wave propagation from the source to the receivers. Time and space steps in AXITRA were four times finer than those of the finite difference grid to insure accurate simulations. We used the crustal model proposed by Husen *et al.* [1999] for Northern Chile.

[10] Synthetic records were compared with real records, using the  $L_2$  norm:

$$\chi^2 = \frac{\sum_i (obs - synth)^2}{\sum_i (obs)^2} \quad (2)$$

where *obs* are the observed displacement and *synth*, the simulated displacement. The sum runs over all samples in every seismogram considered in the inversion. The inver-

sion was made using NA in order to search for the rupture model with minimum misfit. During the inversion many models did not propagate at all, those models have  $\chi^2 = 1$ . Other models produced very fast ruptures that do not fit the data at all, they had  $\chi^2 > 1$ . Once the NA inversion converged, we explored solutions near the minimum using a Monte Carlo (MC) technique. Since we are particularly interested in the friction law, we fixed all the parameters except the applied stress and friction,  $T_e$ ,  $T_u$  and  $D_c$ .

[11] For each model visited in the inversion we computed the seismic moment  $M_0$  and the non-dimensional parameter  $\kappa$ .

$$\kappa = \frac{T_e^2 L}{\mu T_u D_c} \quad (3)$$

Where  $L$ , the characteristic size of the event, is taken as the shorter semiaxis of the source ellipse,  $\mu$  is the shear modulus,  $T_e$ ,  $T_u$  and  $D_c$  were already defined.  $\kappa$  is roughly the ratio of available strain energy to energy release rate, it controls the overall characteristics of the rupture process as discussed by Madariaga and Olsen [2000].

#### 4. Dynamic Inversion Results

[12] The inversions of the asperity and barrier models converged to models that produce a relative residual  $\chi^2$

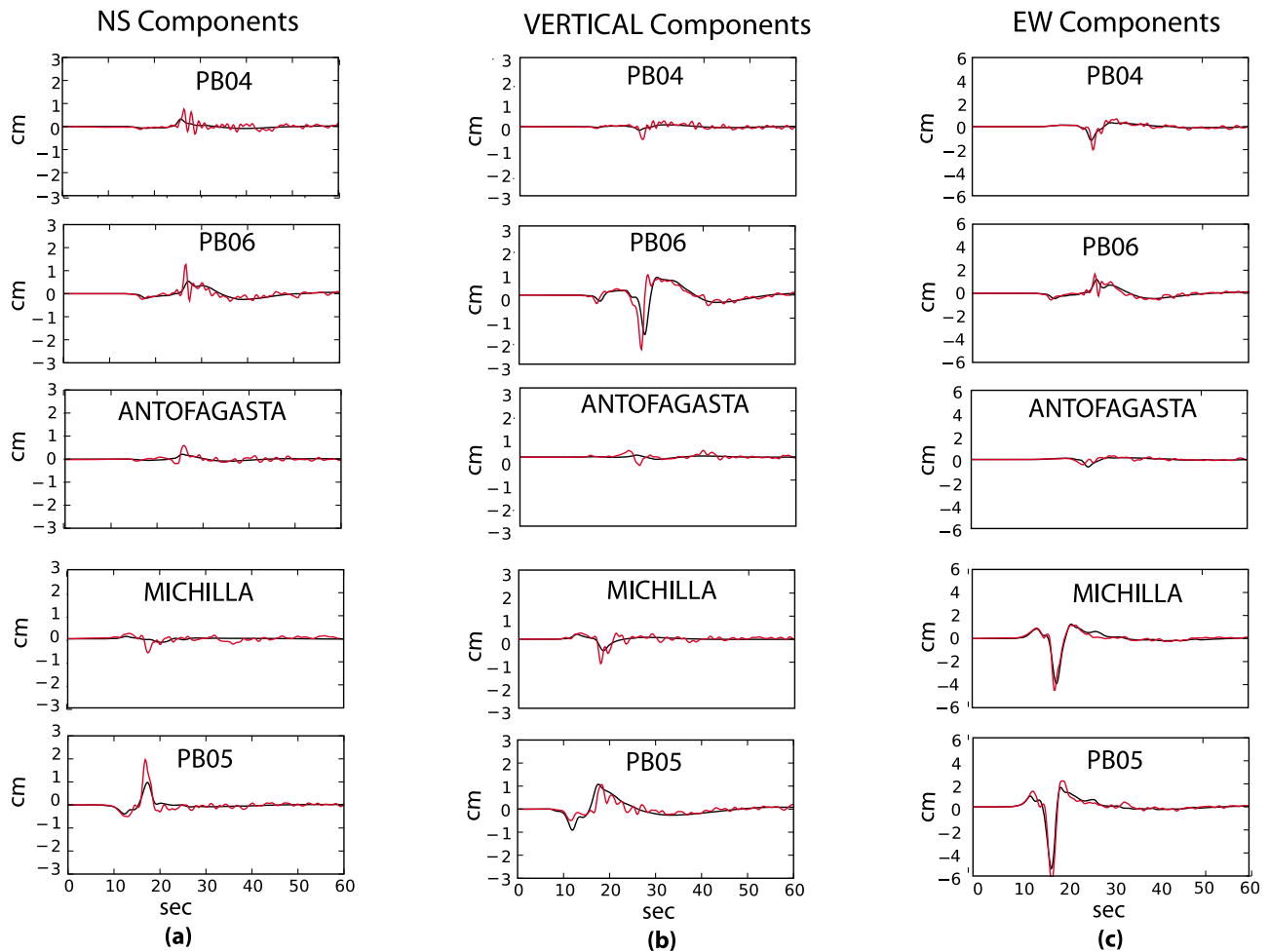


**Figure 3.** Comparison between real (red) and synthetic (black) displacements obtained with the NA inversion algorithm for the asperity model of the 2007 Michilla earthquake. The relative misfit between observed and synthetics was  $\chi^2 = 0.2091$ . (a) EW components, (b) vertical components and (c) NS components.

lower than 0.21. These models had slip and slip rate distributions that were in agreement with the seismic moment, duration and slip distribution expected for an intraplate intermediate depth earthquake of Mw 6.7. Figure 2 shows the slip distribution and rupture time as a function of position on the fault for the best barrier (Figure 2b) and asperity (Figure 2a) models. The ruptures are characterized by a slow initial rupture propagation and large slip in the final part of the rupture. The total duration of the rupture in both cases is less than 5 seconds. The fit between the real and synthetic records is shown in Figure 3 where only the results of the asperity model are shown; similar results were obtained for the barrier model.

[13] Table 1 shows the values obtained for the 11 inverted parameters. Table 2 shows the  $\chi^2$  and  $\kappa$  values obtained for these models. We recall that the critical value for a circular rupture is  $\kappa_c = 0.6$  [Madariaga and Olsen, 2000]. The geometrical parameters are practically the same for the best asperity and barrier models; this is reflected in Figure 2 where the slip distribution and rupture isochrones are very similar for the two models. However, the stress and friction parameters  $T_e$ ,  $T_u$  and  $D_c$  are quite variable. This difference does not affect the slip distribution and rupture time of the

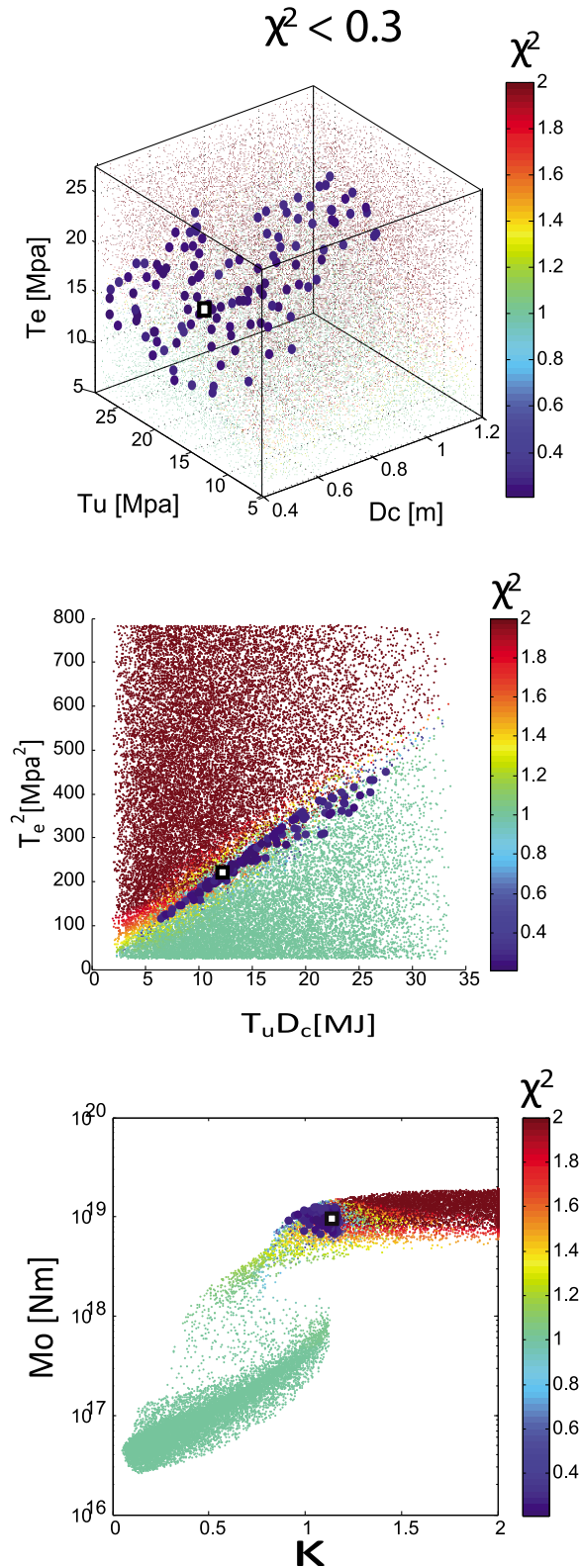
best models, because there is clearly a finite set of models that satisfies the observations.

[14] In order to explore the relation between stress and friction parameters we used the MC method, fixing all the parameters of the models with the exception of  $T_e$ ,  $T_u$  and  $D_c$ . The other parameters were fixed at those of the optimum model in Table 1. The MC inversions allow us to explore the solution space, showing the relations among the stress – friction parameters and how these are related to  $\chi^2$ ,  $M_0$  and  $\kappa$ . Figure 4 (top) shows the results for the MC inversion of the asperity model where more than 30,000 models were simulated, similar results were obtained for the barrier model. In the same manner as for NA, many of the models explored correspond to combination of stress–friction parameters that do not fit the data well. Some have high  $\chi^2$  (small brown dots), others have  $\chi^2$  near to 1 (small green dots). In Figure 4

**Table 2.**  $\kappa$  and  $\chi^2$  Values for the Best Asperity and Barrier Models

Model	$\chi^2$	$\kappa$
Asperity	0.209	1.15
Barrier	0.206	1.11

(top) the best MC models, with misfit  $\chi^2 < 0.3$  are drawn with larger blue dots. These models are located on a rather flat irregular surface of the space  $T_e$ ,  $T_u$  and  $D_c$  (Figure 4, top). As shown in Figure 4 (middle), these models could be collapsed into a single linear structure when the models were projected on the plane  $(T_e^2, T_u D_c)$ . In Figure 4 (middle) the



models with  $\chi^2 < 0.3$  appear as a narrow diagonal band of blue coloured dots. Similar results obtained for other values of  $\chi^2$  are shown in Figure S1 of the auxiliary material.<sup>1</sup>

[15] The alignment of the best models observed in Figure 4 (middle) has a simple interpretation. These models share similar values of  $\kappa$ , the non-dimensional control parameter defined in (3). In Figure 4 (bottom) we plot the models of Figure 4 (top), on the seismic moment vs.  $\kappa$  plane. Figure 4 (bottom) shows that the models with  $\chi^2 < 0.3$  can be grouped in an elongated volume where the seismic moment varies between  $0.4 \cdot 10^{19}$  and  $1.4 \cdot 10^{19}$  Nm and  $\kappa$  varies between  $\kappa = 0.7$  and  $\kappa = 1.2$ . This zone is shown in a different way in Figure S2 of the auxiliary material. The seismic moment associated with the best model inverted by NA was  $0.95 \cdot 10^{19}$  Nm which corresponds to  $M_w = 6.6$ . The models that fit the observations near the optimum form an extended surface that is controlled by the non-dimensional number  $\kappa$  and by the seismic moment that measures the overall slip at the source.

## 5. Discussion and Conclusions

[16] We did a full dynamic inversion of the 16 December 2007 Michilla intermediate depth earthquake for both the asperity and barrier models of seismic rupture. The models were described by 11 parameters. The optimal models had normalized errors  $\chi^2$  lower than 0.21. The slip and slip rate distribution for the best asperity and barrier models are similar, confirming the earlier conjecture that seismic data cannot distinguish between barrier and asperity models [Madariaga, 1979]. The earthquake grew at low initial speed, accelerating near the boundaries of the elliptical rupture. The rupture area is similar to that of the aftershock distributions. The seismic moment was of  $0.95 \cdot 10^{19}$  Nm or  $M_w 6.6$  slightly less than the  $M_w 6.8$  found by Peyrat *et al.* [2010].

[17] We explored the parameters of the friction law around the best solution using a MC technique fixing the geometrical parameters. We looked for the combination of stress and friction parameters that produced models that fit the data with relative errors of less than 30%. We found that these solutions form a narrow irregular surface when the solutions were projected into the  $T_e^2$  vs  $T_u D_c$  plane. This is a

<sup>1</sup>Auxiliary materials are available in the HTML. doi:10.1029/2011GL047147.

**Figure 4.** Study of the stress and friction parameters by Monte Carlo inversion. In all the plots, each dot corresponds to one simulated model. The larger points have a relative error  $\chi^2 < 0.3$ . The color scale is saturated for misfits  $\chi^2 \geq 2$ . The black square corresponds to the optimum solution determined by NA (lowest  $\chi^2$ ) (top) Plot of error for each model projected onto the  $D_c, T_e, T_u$ , plane. Dots are coloured according to the value of  $\chi^2$  as indicated in the colour bar. Models with  $\chi^2 < 0.3$  form a narrow irregular surface. (middle) The models are projected on the plane  $T_e^2$  versus  $T_u D_c$ . Models with  $\chi^2 < 0.3$  are plotted with bigger blue dots; they form a narrow elongated structure that indicates that these models share a common non-dimensional number  $\kappa$ . (bottom) Model relative error  $\chi^2$  plotted as a function of the global parameters seismic moment and  $\kappa$ . The better models form a narrow zone in the  $M_0, \kappa$  plane (blue dots).

clear indication that good solutions of the inverse problems are actually controlled by seismic moment and  $\kappa$ . Models with misfit  $\chi^2 < 30\%$  belong to a narrow range of  $\kappa$  values between 0.7 and 1.2. Our results clearly show that seismic observations are compatible with a certain range of frictional and stress parameters determined by the seismic moment of the event and  $\kappa$ . We chose the Michilla earthquake because it had a simple rupture surface as determined from kinematic inversions by Peyrat *et al.* [2010]. For more complex events a single ellipse will not be sufficient to describe its geometry but we expect the main result to remain valid: it is possible to estimate the friction law from seismic observations but there are clear tradeoffs between stress and friction.

[18] **Acknowledgments.** This work was supported by FONDECYT 1100429 in Chile and by ANR DEBATE in France. Sergio Ruiz was partially supported by the Nucleo Milenio IERC-MB. We thank B. Schurr and other colleagues at GFZ who deployed the plate boundary stations in Northern Chile (PBs); Frank Scherbaum of GFZ and R. Boroschek of Universidad de Chile for the accelerograms. We sincerely thank M. Lancieri, J. Campos, A. Fuenzalida, S. Peyrat and J. P. Vilotte for their help and advice.

[19] Finally, we thank Ruth Harris and two anonymous referees for their very useful and constructive reviews. The Editor thanks Andrea Bizzarri and an anonymous reviewer for their assistance in evaluating this paper.

## References

- Bizzarri, A. (2009), What does control earthquake ruptures and dynamic faulting? A review of different competing mechanisms, *Pure Appl. Geophys.*, *166*(5–7), 741–776, doi:10.1007/s00024-009-0494-1.
- Bouchon, M. (1981), A simple method to calculate Green's functions for elastic layered media, *Bull. Seismol. Soc. Am.*, *71*, 959–971.
- Bouchon, M., M. Campillo, and F. Cotton (1998), Stress field associated with the rupture of the 1992 Landers, California, earthquake and its implication concerning the fault strength at the onset of the earthquake, *J. Geophys. Res.*, *103*, 21,091–21,097, doi:10.1029/98JB01982.
- Coutant, O. (1990), Programme de simulation numerique AXITRA, Rapport LGIT, Univ. Joseph Fourier, Grenoble, France.
- Das, S., and K. Aki (1977), Fault plane with barriers-versatile earthquake model, *J. Geophys. Res.*, *82*, 5658–5670, doi:10.1029/JB082i036p05658.
- Delouis, B., M. Pardo, D. Legrand, and T. Monfret (2009), The Mw7.7 Tocopilla earthquake of 14 November 2007 at the southern edge of the Northern Chile seismic gap: Rupture in the deep part of the coupled plate interface, *Bull. Seismol. Soc. Am.*, *99*, 87–94, doi:10.1785/0120080192.
- Di Carli, S., C. Francois-Holden, S. Peyrat, and R. Madariaga (2010), Dynamic inversion of the 2000 Tottori earthquake based on elliptical subfault approximations, *J. Geophys. Res.*, *115*, B12328, doi:10.1029/2009JB006358.
- Fukuyama, E., and T. Mikumo (1993), Dynamic rupture analysis: Inversion for the source process of the 1990 Izu Oshima, Japan earthquake (M6.5), *J. Geophys. Res.*, *98*, 6529–6542, doi:10.1029/92JB02451.
- Guatteri, M., and P. Spudich (2000), What can strong-motion data tell us about slip-weakening fault friction laws?, *Bull. Seismol. Soc. Am.*, *90*, 98–116, doi:10.1785/0119990053.
- Husen, S., E. Kissling, and G. Asch (1999), Accurate hypocentre determination in the seismogenic zone of the subducting Nazca plate in northern Chile using a combined on-/off-shore network, *Geophys. J. Int.*, *138*, 687–701, doi:10.1046/j.1365-246x.1999.00893.x.
- Ida, Y. (1972), Cohesive force across tip of a longitudinal-shear crack and Griffith specific surface-energy, *J. Geophys. Res.*, *77*, 3796–3805, doi:10.1029/JB077i020p03796.
- Kanamori, H., and G. S. Stewart (1978), Seismological aspects of the Guatemala earthquake of February 4, 1976, *J. Geophys. Res.*, *83*, 3427–3434, doi:10.1029/JB083iB07p03427.
- Madariaga, R. (1979), On the relation between seismic moment and stress drop in the presence of stress and strength heterogeneity, *J. Geophys. Res.*, *84*, 2243–2250, doi:10.1029/JB084iB05p02243.
- Madariaga, R., and K. B. Olsen (2000), Criticality of rupture dynamics in 3-D, *Pure Appl. Geophys.*, *157*, 1981–2001, doi:10.1007/PL00001071.
- Madariaga, R., K. B. Olsen, and R. Archuleta (1998), Modeling dynamic rupture in a 3D earthquake fault model, *Bull. Seismol. Soc. Am.*, *88*, 1182–1197.
- Peyrat, S., and K. B. Olsen (2004), Nonlinear dynamic rupture inversion of the 2000 Western Tottori, Japan, earthquake, *Geophys. Res. Lett.*, *31*, L05604, doi:10.1029/2003GL019058.
- Peyrat, S., K. Olsen, and R. Madariaga (2001), Dynamic modeling of the 1992 Landers earthquake, *J. Geophys. Res.*, *106*, 26,467–26,482, doi:10.1029/2001JB000205.
- Peyrat, S., R. Madariaga, E. Buforn, J. Campos, G. Asch, and J. P. Vilotte (2010), Kinematic rupture process of the 2007 Tocopilla earthquake and its main aftershocks from teleseismic and strong-motion data, *Geophys. J. Int.*, *182*, 1411–1430, doi:10.1111/j.1365-246X.2010.04685.x.
- Piatanesi, A., E. Tinti, M. Cocco, and E. Fukuyama (2004), The dependence of traction evolution on the earthquake source time function adopted in kinematic rupture models, *Geophys. Res. Lett.*, *31*, L04609, doi:10.1029/2003GL019225.
- Sambridge, M. (1999), Geophysical inversion with a neighbourhood algorithm—I. Searching a parameter space, *Geophys. J. Int.*, *138*, 479–494, doi:10.1046/j.1365-246X.1999.00876.x.
- Schurr, B., A. Asch, F. Sodoudi, A. Manzanares, O. Ritter, J. Klotz, G. Chong-Diaz, S. Barrientos, J.-P. Vilotte, and O. Oncken (2009), The International Plate Boundary Observatory Chile (IPOC) in northern Chile seismic gap, Abstract EGU2009-11040 presented at General Assembly 2009, Eur. Geosci. Union, Vienna, 19–24 April.
- Sobiesiak, M., S. Eggert, H. Grosse, T. Walter, B. Schurr, J. P. Vilotte, C. Arranda, H. Woith, H. U. Wetzel and G. Gonzales (2008), Post seismic task force operation after the Mw 7.7 Tocopilla earthquake in northern Chile, Abstract EGU2008-A-09928 presented at General Assembly 2008, Eur. Geosci. Union, Vienna, 13–18 April.

R. Madariaga, Laboratoire de Géologie, Ecole Normale Supérieure, 24 rue Lhomond, F-75231 Paris CEDEX 05, France. (madariag@geologie.ens.fr)  
S. Ruiz, Departamento de Geología, Universidad de Chile, Av. Blanco Encalada 2002, Santiago, Chile. (sruiz@ing.uchile.cl)